Interatomic repulsion softness directly controls the fragility of supercooled metallic melts

Johannes Krausser[a,b], Konrad H. Samwer[c], and Alessio Zaccone[a,b,1]

[a]Physics Department and Institute for Advanced Study, Technische Universität München, 85748 Garching, Germany; [b]Department of Chemical Engineering and Biotechnology, University of Cambridge, Cambridge CB2 3RA, United Kingdom; and [c]I. Physikalisches Institut, Universität Göttingen, 37077 Göttingen, Germany

Edited by Michael L. Falk, Johns Hopkins University, Baltimore, MD, and accepted by the Editorial Board September 22, 2015 (received for review February 24, 2015)

We present an analytic scheme to connect the fragility and viscoelasticity of metallic glasses to the effective ion–ion interaction in the metal. This is achieved by an approximation of the short-range repulsive part of the interaction, combined with nonaffine lattice dynamics to obtain analytical expressions for the shear modulus, viscosity, and fragility in terms of the ion–ion interaction. By fitting the theoretical model to experimental data, we are able to link the steepness of the interionic repulsion to the Thomas–Fermi screened Coulomb repulsion and to the Born–Mayer valence electron overlap repulsion for various alloys. The result is a simple closed-form expression for the fragility of the supercooled liquid metal in terms of few crucial atomic-scale interaction and anharmonicity parameters. In particular, a linear relationship is found between the fragility and the energy scales of both the screened Coulomb and the electron overlap repulsions. This relationship opens up opportunities to fabricate alloys with tailored thermoelasticity and fragility by rationally tuning the chemical composition of the alloy according to general principles. The analysis presented here brings a new way of looking at the link between the outer shell electronic structure of metals and metalloids and the viscoelasticity and fragility thereof.

metallic glasses | fragility of liquids | supercooled liquids | glass transition | liquid metals

Understanding the mechanism which governs the emergence of mechanical stability at the glass transition of supercooled metallic liquids (1) calls for deeper insights into the connection between the fragility index and the interatomic interaction. As previous work suggested (2–4), mechanical stability in amorphous solids is crucially linked to the repulsive part of the interatomic interaction potential. However, no consensus has been reached on whether interatomic repulsion softness correlates with strong glasses (5) or with fragile glasses (6). We derive an analytical closed-form relation between the fragility index of metallic glass formers and the short-ranged repulsive part of the interatomic interaction given by pseudopotential theory. This fundamental relation is obtained from a one-parameter theory fit to experimental rheological data of supercooled metallic melts. Resorting to this combination of theory and experiments, it is established that interatomic repulsion softness in metals goes along with strong glasses and low fragility. Surprisingly, given the difference in energy scale of many orders of magnitude and the nature of the microscopic interaction, this finding is in full agreement with the correlation observed experimentally for soft colloidal glasses by Mattsson, Weitz, and coworkers (5). Finally, we establish a quantitative link between our analysis and the theory of shear transformation zones to estimate the size of the cooperatively rearranging regions in good agreement with the findings in ref. 7.

Shear Modulus of Glasses

The starting point for linking the shear modulus and the atomic connectivity analytically is the theoretical framework of nonaffine elastic response (8–10). The standard affine approximation of the classical Born–Huang theory is not applicable to amorphous as well as other noncentrosymmetric lattices (11). This problem arises due to the lack of local inversion symmetry in amorphous solids. As a consequence, the deformation forces which are transmitted to an atom by its bonded neighbors do not balance each other by mirror symmetry. The resulting forces, which act on every atom, are released through additional nonaffine motions on top of the standard affine displacements dictated by the macroscopic strain. In other words, the continuum assumption that the macroscopic deformation scales down to the microscopic lattice does not generally hold for amorphous systems.

Structural disorder and nonaffine motions can be taken into account using the theory of nonaffine elastic response. For an amorphous solid under a shear strain γ, we can express the free energy of deformation as $F(\gamma) = F_{\mathrm{A}}(\gamma) - F_{\mathrm{NA}}(\gamma)$ (12). The two terms represent the standard affine contribution to the free energy, provided by the framework of Born–Huang lattice dynamics (13, 14), and the nonaffine contribution, respectively. Resorting to an eigenfunction decomposition of the nonaffine contribution, it is possible to derive an analytic expression for the shear modulus of an amorphous lattice. This has been done for example by Lemaître and Maloney (8), and the result for the shear modulus is given by

$$G = G_{\mathrm{A}} - G_{\mathrm{NA}} = G_{\mathrm{A}} - \sum_{i,j} \underline{f}_i^T \, \underline{\underline{H}}_{ij}^{-1} \underline{f}_j, \qquad [1]$$

where $\underline{\underline{H}}_{ij} = (\partial^2 U / \partial \underline{r}_i \partial \underline{r}_j)_{\gamma \to 0}$ represents the standard dynamical matrix of the solid (15), U is the internal energy of the system, and $\underline{f}_i$ is the force per unit strain acting on the atoms due to the shear deformation (8). The explicit expression for the affine contribution to the shear modulus is given by $G_{\mathrm{A}} = (N/30V)\kappa R_0^2 Z$,

Significance

Bulk metallic glasses are the most promising materials in many technological applications thanks to their mechanical properties. The stability and thermoelasticity of supercooled liquid metals is encoded in the temperature dependence of the viscosity at the glass transition: the fragility. Although with colloidal glasses it has been possible to explain the fragility in terms of the softness (or its inverse, the steepness) of the microscopic interparticle potential, the same could not be done with metals due to the complex interatomic interaction. Here we solve this problem and propose a new methodology which provides the missing analytical link between fragility and interatomic potential in metals. Our results show that the same scenario found earlier with colloidal glasses applies to metals too.

Author contributions: K.H.S. and A.Z. designed research; J.K. and A.Z. performed research; J.K., K.H.S., and A.Z. analyzed data; and J.K. and A.Z. wrote the paper.

The authors declare no conflict of interest.

This article is a PNAS Direct Submission. M.L.F. is a guest editor invited by the Editorial Board.

[1]To whom correspondence should be addressed. Email: az302@cam.ac.uk.

This article contains supporting information online at www.pnas.org/lookup/suppl/doi:10.1073/pnas.1503741112/-/DCSupplemental.

which is discussed in *Supporting Information*. As shown in ref. 9, assuming a central force interaction and introducing the atomic packing fraction $\phi = vN/V$, with v a characteristic rigid core volume, Eq. **1** can be evaluated analytically as

$$G = G_A - G_{NA} = \frac{1}{5\pi}\frac{\kappa}{R_0}\phi(Z - Z_c). \quad [2]$$

The nonaffinity of the amorphous solid is encoded in the quantity $-Z_c$, which denotes the critical number of bonds at which the shear modulus vanishes by virtue of the nonaffine softening mechanism. This expression still does not include the direct contribution of thermal effects to the elastic response. Thermal vibrations, in fact, soften the shear modulus by an additional negative term $-3(N/V)kT\partial^2(\ln\hbar\omega/kT)/\partial\gamma^2$ (9, 16). For many materials, including metallic and polymer materials, this contribution is very small compared with the other terms in Eq. **2**. It determines a decreasing trend of G with T which is negligible compared with the combined effect of nonaffinity and thermal expansion (17).

Temperature Dependence of the Shear Modulus

The crucial effect which controls the temperature dependence of the shear modulus is the change in atomic connectivity Z due to Debye–Grüneisen thermal expansion (9). Approaching the glass transition temperature T_g from below, this effect is responsible for the loss of mechanical stability. We will show that the same effect is responsible for the decrease of the high-frequency shear modulus with increasing T in the supercooled liquid above T_g.

The atomic packing fraction ϕ is reduced upon increasing the temperature T, an effect mediated by the thermal expansion coefficient defined as $\alpha_T = \frac{1}{V}(\partial V/\partial T) = -\frac{1}{\phi}(\partial\phi/\partial T)$. Integrating this, we see that the atomic packing fraction evolves with T according to $\log(1/\phi) = \alpha_T\, T + c$. For an amorphous metal, a decrease in Z arises if the separation between two particles is larger than the typical length scale of attraction defined by the first minimum of the interatomic pseudopotential r_{min}. For example, if the separation of an atom from one of its caged nearest-neighbors exceeds $r > r_{min}$, the neighbor effectively leaves the coordination shell or cage (9) and no longer contributes to the cage elasticity.

When increasing T, the average spacing between atoms in the coordination shell becomes larger, and the probability of nearest neighbors leaving the connectivity shell increases. It is then possible to use the radial distribution function $g(r)$ to relate the change in packing fraction $\delta\phi$, due to an externally imposed change in temperature δT, to the change in connectivity δZ. Following along the lines of ref. 9, the change of atomic connectivity $\delta Z = Z - Z_c$, relative to the critical stability (isostatic) point Z_c, can be calculated when the density of the system increases by an increment $\delta\phi = \phi - \phi_c$ according to

$$Z - Z_c \sim \int_1^{1+\delta\phi} r^2 g(r)\mathrm{d}r, \quad [3]$$

where r represents a dimensionless distance defined with respect to the rigid core diameter σ. Because the radial distribution function $g(r)$ is not known in analytical form for real materials, we introduce an approximation scheme. The basic idea is to represent the repulsive side of the first peak of $g(r)$ by means of the power law approximation $g(r) \sim (r-\sigma)^{\lambda}$. In this way, the parameter λ uniquely characterizes the steepness of the left-hand side of the first peak of the radial distribution function. The dashed lines shown in Fig. 1*A* represent the power law approximation to the actual radial distribution function.

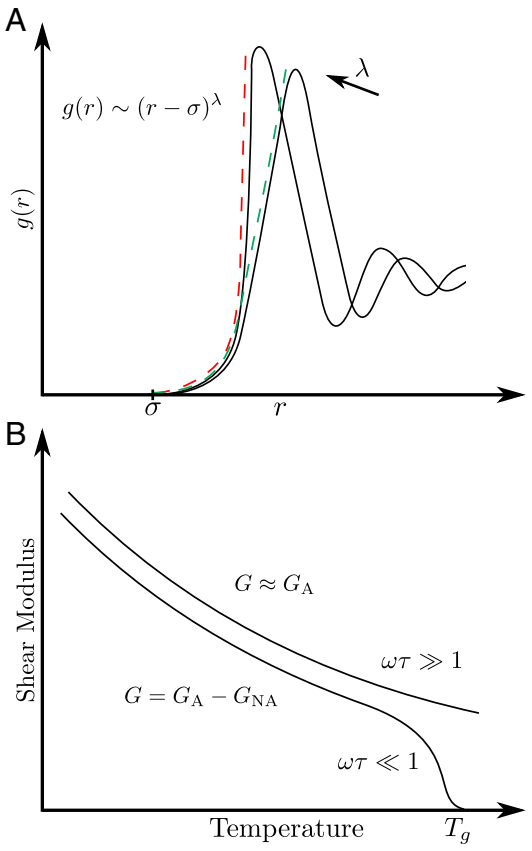

Fig. 1. (*A*) Approximation of the repulsive part of the first peak of $g(r)$ using two different values for the steepness λ. An increase in λ is linked to a steeper slope of $g(r)$. (*B*) In the high-frequency regime the affine shear modulus represents a good approximation to the actual behavior of the shear modulus $G = G_A - G_{NA}$.

We know that the potential of mean force (18) between two atoms is related to the radial distribution function by $V_m/kT = -\ln g(r) \sim -\ln(r-\sigma)^{\lambda}$, where the ion core diameter σ indicates the mutual separation between two ions at which the interaction energy is practically infinite. If the separation between two ions is small, V_m reduces to the short-range part of the ion–ion repulsion. Hence, λ is proportional to the steepness of the short-range effective repulsion and inversely proportional to the softness of the pseudopotential, which scales as $1/\lambda$.

Subsequently, with the power law approximation for $g(r)$ in Eq. **3**, the change in connectivity becomes a function of the repulsion steepness λ: $\delta Z \sim \delta\phi^{1+\lambda}$. It is assumed that the spherical integration is well approximated by Cartesian coordinates at short separations. When decreasing the temperature by $\delta T < 0$, the atomic packing fraction grows by $\delta\phi = -\phi\alpha_T\delta T > 0$. Consequently, the connectivity Z increases more strongly for steeper pseudopotentials than for the softer counterpart. Analogously, an increase of temperature, $\delta T > 0$, causes the atomic connectivity to decrease more abruptly with T for a steep ion–ion repulsion and more gradually for a softer interaction.

The High-Frequency Shear Modulus

Experimental measurements of the viscosity and shear modulus of supercooled liquid metals at the glass transition can be obtained using ultrasonic techniques, which probe the material response at frequencies in the GHz range (19). These high frequencies exceed the typical relaxation frequency of a metallic glass by several orders of magnitude (20). Under such conditions, the response to an applied oscillatory shear strain generally is dominated by

Table 1. Summary of the experimental data

Alloy	T_g, K	$10^2\alpha_T T_g$	λ	C_G, GPa	V_c, 10^{-27}m^3	$m(\lambda)$	m
$Zr_{46.75}$ $Ti_{8.25}$ Ni_{10} $Cu_{7.5}$ $Be_{27.5}$	597 (19)	0.591	99.7	34.52	—	—	—
Pd_{43} Cu_{27} Ni_{10} P_{20}	567 (19)	0.935 (39)	115.9	30.44	—	—	—
$Pt_{57.5}$ $Ni_{5.3}$ $Cu_{14.7}$ $P_{22.5}$	489 (19)	0.776	164.2	30.56	—	—	—
La_{55} Al_{25} Ni_{20}	465 (39)	0.711 (39)	196.2	15.4 (20)	0.0148	37.16	37_{450K} (19) 33_{462K} (40)
$Zr_{41.2}$ $Ti_{13.8}$ Ni_{10} $Cu_{12.5}$ $Be_{22.5}$	623 (39)	0.617 (39)	276.4	33.2 (19)	0.0085	38.74	40_{613K} (19) 39_{648K} (41)
Pd_{40} Ni_{40} P_{20}	551 (39)	0.856 (39)	286.5	36.5 (20)	0.0069	49.91	50_{560K} (19) 41_{580K} (42)
$Pd_{77.5}$ Cu_6 $Si_{16.5}$	625 (39)	0.865 (39)	381.2	32.9 (20)	0.0084	60.04	61_{634K} (19) 52_{635K} (42)

the instantaneous (affine or quasi-affine) limit of the shear modulus. For frequencies ω much larger than the inverse of the Maxwell relaxation time τ, that is for $\omega\tau \gg 1$, the shear modulus cannot decay through a nonaffine relaxation process. This situation is sketched in Fig. 1*B* together with the low-frequency case, where the nonaffine decay is possible.

At high frequency, the atoms cannot leave their affine positions to reach the nonaffine positions because the deformation is too quickly reverted. Hence, the elastic response at GHz frequencies is predominantly affine, as shown in *Supporting Information* using the full nonaffine response theory. Considering Eq. **2**, this means that the shear modulus is reduced to its affine contribution in the sense that $G \overset{\omega\to\infty}{\longrightarrow} G_A$. Consequently, in this regime the expression for G is proportional to Z (13) but no longer depends on the critical connectivity Z_c. Therefore, it holds true that $\delta Z \to Z$ and $\delta\phi \to \phi$. Setting Z_c and ϕ_c to zero is the defining feature of the high-frequency quasi-affine limit (14).

Going back to Eq. **1**, we recognize that in the regime $\omega\tau \gg 1$ this leaves us with $G = \frac{1}{5\pi}\frac{\kappa}{R_0}\phi Z$. We recall that the packing fraction depends on T, $\phi(T) \sim e^{-\alpha_T T}$, and thus, we obtain $Z(T) \sim e^{-(1+\lambda)\alpha_T T}$. Upon replacing this result in the above equation for G, we find that the T dependence of the shear modulus is dictated by

$$G(T) \sim \frac{1}{5\pi}\frac{\kappa}{R_0}\exp[-(2+\lambda)\alpha_T T]. \qquad [4]$$

The high-frequency shear modulus now explicitly depends on the softness of the interaction potential and on the thermal expansion coefficient α_T. Both these crucial effects are reflections of the anharmonicity of the elastic response.

As already hinted above, we remark that in general there is also a phonon contribution to the shear modulus proportional to $kTe^{-\alpha_T T}$. However, this contribution is typically negligible with respect to the one in Eq. **4** (17), even more so if one considers, as it will be shown below, that typical values of λ are in the range 100–400.

Comparison with Experimental Data

The above expression for the high-frequency affine shear modulus can be rewritten as

$$G(T) = C_G \exp\left[\alpha_T T_g(2+\lambda)\left(1-\frac{T}{T_g}\right)\right], \qquad [5]$$

where $C_G = \frac{\varepsilon}{5\pi}\frac{\kappa}{R_0}e^{-\alpha_T T_g(2+\lambda)}$ is a prefactor independent of T. The constant ε stems from the integration of α_T and from the dimensional prefactor in the power law ansatz for $g(r)$. All of the parameters in this expression, which are given in Table 1, are fixed by the experimental protocol, apart from the fitting parameter λ related to the ion–ion repulsion steepness. With Eq. **5** at hand, we can generate a one-parameter fit to the experimental data provided from ref. 19, which accurately captures the datasets for the three metallic glass alloys, as can be seen from Fig. 2*A*. The different slope of the three depicted curves reflects the fact that the repulsion steepness λ in Eq. **5** controls the behavior of $G(T)$. A decreasing λ, among the different alloys, correlates with a slower decrease of the shear modulus upon increasing the temperature.

Furthermore, we can use our model for the high-frequency shear modulus to evaluate the activation energy $E(T)$ involved in restructuring the glassy cage and, hence, the viscosity η of the melts. Within the framework of the shoving or elastic model of the glass transition (21–24), the activation energy for local cooperative rearrangements is $E(T) = G_A V_c$. The characteristic atomic volume V_c appearing here is accessible through the theoretical fitting to the viscosity data, although its value is approximately specified by the atomic composition of the alloy.

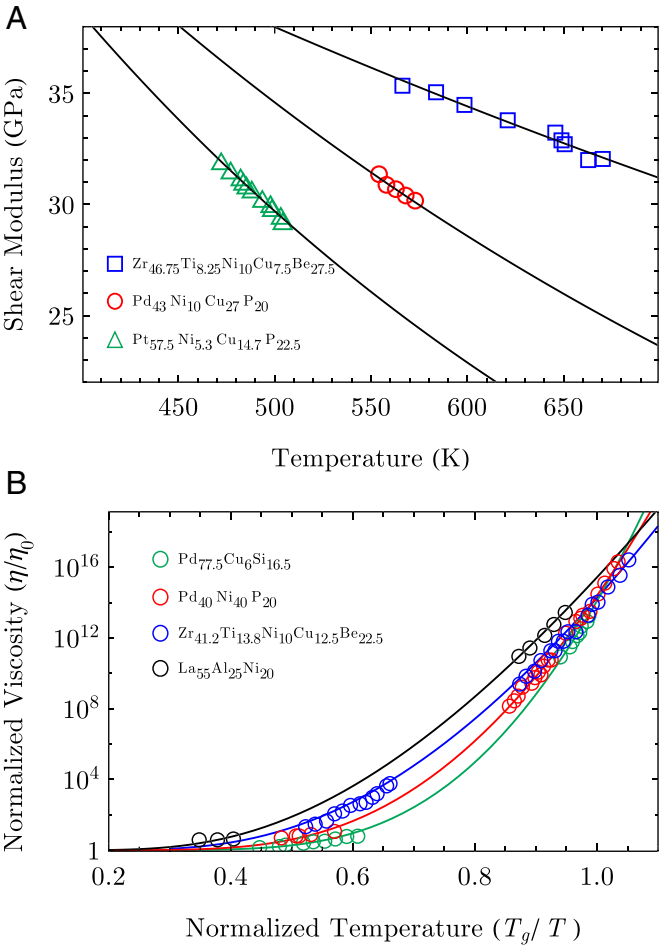

Fig. 2. The experimental data points for various glass-forming alloys from ref. 19 and the respective fitting curves for the shear modulus in *A* and the viscosity in *B*. The solid lines are the one-parameter fitting curves obtained using the expressions in Eqs. **5** and **6**, for the shear modulus and viscosity, respectively. The values used for the fittings are reported in Table 1.

Replacing the expression for the activation energy in the Arrhenius relation given by the shoving model of the glass transition and using Eq. **5** for the high-frequency shear modulus G_A inside $E(T)$, we obtain the following analytical expression for the viscosity:

$$\frac{\eta(T)}{\eta_0} = \exp\left\{\frac{V_c C_G}{kT}\exp\left[(2+\lambda)\alpha_T T_g\left(1-\frac{T}{T_g}\right)\right]\right\}, \qquad [6]$$

where η_0 is a normalization constant.

It is important to note how the double-exponential of the viscosity versus T arises. The first exponential stems from the elastic activation described in the framework of the shoving model, whereas the second exponential is due to the Debye–Grüneisen thermal expansion rooted in lattice-dynamical considerations and ultimately related to anharmonicity.

We compare the theoretical predictions to the experimental data of ref. 19 in Fig. 2*B*. In this case there is also an excellent agreement between theory and experiment with the adjustable parameters being λ, the steepness of the short-ranged ion–ion repulsion, and V_c, the characteristic atomic volume.

Interatomic Repulsion and Fragility

With the analytical theory developed above, we are in the position to relate the atomic-scale properties of the interaction between ions to the experimentally observable macroscopic response of the material. We now consider the behavior of the viscosity in Fig. 2*B* together with the corresponding behavior of the interaction parameter λ for various alloys in Table 1. Evidently, upon approaching the glass transition, the slope of the viscosity $\eta(T)$ is controlled by the interatomic repulsion steepness λ, which depends on the atomic composition of the alloy. A steeper pseudopotential repulsion between two nearest-neighbor ions goes hand in hand with a steeper rise of viscosity, when T is increased.

This observation leads us straight to connecting the softness of the potential to the fragility of metallic glasses. The fragility is given as the slope of the viscosity evaluated at the glass transition temperature T_g, i.e., $m = \left(\frac{\partial \log_{10}(\eta/\eta_0)}{\partial(T_g/T)}\right)\Big|_{T=T_g}$ (25). Using the analytical expression for η, Eq. **6**, we obtain a simple relation between the fragility m and the steepness of the interatomic repulsion λ given by

$$m(\lambda) = \frac{1}{\ln 10}\frac{V_c C_G}{kT_g}\left[1+(2+\lambda)\alpha_T T_g\right]. \qquad [7]$$

Metallic glasses with a steeper repulsive part of the interatomic interaction are thus more fragile. The values of the fragility obtained for the various alloys of ref. 19 are listed in Table 1, together with the fitted values of the interatomic repulsion steepness λ. Good agreement is also found with independent experimental measurements of m from the literature.

This prediction is in full agreement with the experimental findings of ref. 5. In that work the softness of the interparticle potential was varied in a model colloidal glass, where the energy scale is orders of magnitude smaller than in metals.

The model also can capture the behavior of m observed in simulation studies of Lennard–Jones glasses, where the attractive anharmonicity controls the fragility via the thermal expansion coefficient, and by construction, a high anharmonicity is accompanied by a low repulsion steepness (26).

Extracting Pseudopotentials from Experimental Data

Given the schematic form of the repulsive short-range part of the interaction, $-\ln(r-\sigma)^{\lambda}$, used in the fitting, it is desirable to map this semiempirical repulsion onto a physically realistic interatomic pseudopotential. This can be achieved by using an Ashcroft-type pseudopotential for modeling the Thomas–Fermi screened interionic

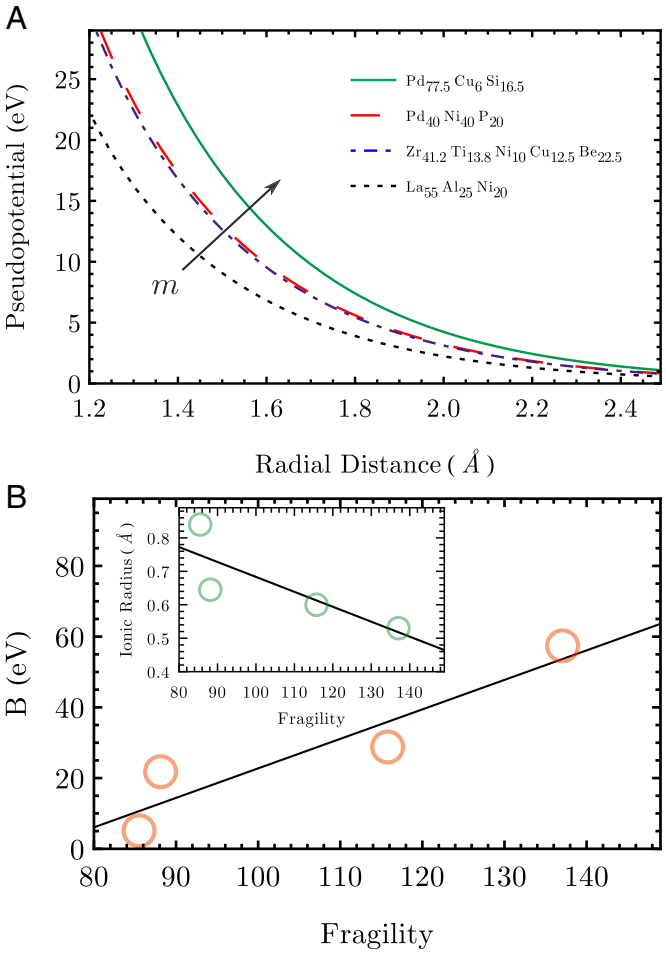

Fig. 3. (*A*) The Ashcroft–Born–Mayer pseudopotential is depicted for four different glass-forming alloys. The fragility m increases with the pseudopotential steepness. (*B*) The value of the Born–Mayer energy scale increases linearly with the fragility. Also, it is observed that the average ionic diameter decreases linearly with the fragility.

Coulomb repulsion (27) and, in addition, a Born–Mayer interaction term which accounts for the effect of electron overlap and Pauli exclusion repulsion between valence electron shells of two interacting ions (28). A more detailed discussion of this matter can be found in *Supporting Information*. This combination of the two contributions to the interaction is the most meaningful choice for the present situation, as discussed in ref. 29.

The softness of the pseudopotential is predominantly controlled by the Born–Mayer parameters because electron overlap repulsion between valence electrons is more energetic over a broader length scale compared with the Ashcroft contribution, as illustrated in *Supporting Information*. Physically, a slower decay of the electron overlap repulsion with distance reflects the softness of the effective interaction. The glass stability, however, is optimized by the coexistence of both softness and substantial repulsion, as is the case for technologically important alloys, like binary Zr-Cu alloys (30).

Microscopically, it is the strongly anisotropic density distribution of d-shell electrons, due to the quadrupolar d-wave symmetry, which provides significant softness (upon taking a spherical average), compared with the more isotropic electron density distribution of elements whose outer shells are dominated by s-electrons. Hence, the form of the pseudopotentials may explain the difference in stability and fragility based on the composition of the alloy. In our model, this effect is expressed by the energy scale of the Born–Mayer repulsion B. In particular, we find that B correlates

linearly with the fragility index m, as shown in Fig. 3*B*. This correlation reflects the fact that d-shell orbitals effectively soften the interatomic repulsion, whereas s-shell electrons are associated with steeper repulsion and higher fragility.

The second effect which is captured by this approach is the ion size mismatch. If smaller metal atoms are added to larger atoms, fragility decreases and strong glasses can be formed. This mechanism which affects multicomponent alloys is analyzed and discussed in ref. 31. Again, this is the consequence of an effectively softer interatomic repulsion. Smaller atoms of metalloids like P, B, or Si can easily come closer to larger ions like Pd, La, Zr, or Cu by fitting into the voids of the quadrupolar d-shell structure. In general, this topological effect also leads to a softer average pseudopotential.

This connection between macroscopic flow behavior, encoded in m, and electronic structure is an important step toward a unifying framework for understanding and controlling mechanical properties of metallic glasses on the atomic scale.

Connection with Cooperative Shear Events

As already pointed out, the energy necessary to trigger a shoving event is $E(T) = G_A(T)V_c$. The characteristic atomic volume V_c is not the volume change which is connected to a shoving event. This quantity, also called the activation volume ΔV, is connected to V_c and the initial shoving volume V via the relation

$$V_c = \frac{2}{3}\frac{(\Delta V)^2}{V}, \qquad [8]$$

which can be derived in the framework of the elasticity theory of an isotropic expanding sphere (23).

It is widely believed that shear transformation zones (STZs) are the fundamental plastic entities responsible for the yielding mechanism in metallic glasses. STZs are clusters of atoms which can cooperatively rearrange under shear stress and are directly connected to the local accumulation of free volume (32). It is in this sense that the activation of STZs allows the involved atoms to rearrange more easily under shear stress. Assuming that the initial shoving volume V corresponds to the volume of a STZ, we find a direct relation between the characteristic volume V_c and the activation volume ΔV in the following way.

According to ref. 33, the total energy barrier W between two basins in the potential energy landscape can be evaluated to give $W \approx (1/320)\ G_A\Omega$ (*Supporting Information*). We assume that W in the cooperative shear model is approximately equal to the shoving energy, that is, $W \approx E$. It directly follows that $G_A V_c \approx (1/320) G_A \Omega$, which leads us to conclude that the effective volume of a STZ is $\Omega \approx 320 V_c$.

It is physically meaningful that the effective STZ volume Ω is approximately equivalent to the initial shoving volume V, henceforth calling it V_{STZ}. Using the identification $\Omega \approx V_{STZ} \approx 320 V_c$, we can use the values for V_c to extract values for STZ volumes from our theoretical analysis and compare them to experimental results for V_{STZ} from ref. 7. We find that the calculated STZ volumes for the respective alloys are in very good agreement with the experimental results for similar alloys, which is displayed in Table 2.

Table 2. Experimental and theoretical STZ volumes

Alloy	V_c, nm^3	Ω, nm^3
$Pd_{40}\ Ni_{40}\ P_{20}$	0.0069	2.21
$Pd_{48}\ Ni_{32}\ P_{20}$	—	2.36 (7)
$Zr_{41.2}\ Ti_{13.8}\ Ni_{10}\ Cu_{12.5}\ Be_{22.5}$	0.0085	2.72
$Zr_{46.75}\ Ti_{8.25}\ Ni_{10}\ Cu_{7.5}\ Be_{27.5}$	—	3.13 (7)
$La_{55}\ Al_{25}\ Ni_{20}$	0.0148	4.74
$La_{55}\ Al_{25}\ Ni_{20}$	—	5.31 (7)

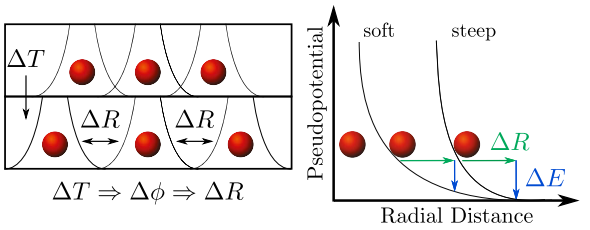

Fig. 4. (*Left*) The distance between the atoms decreases as the temperature is increased, leading to a smaller overlap of the effective interaction potentials. (*Right*) The growth of the cage by ΔR when increasing the temperature by ΔT and the corresponding loss of stabilizing energy ΔE. The potentials are shifted for the sake of clarity.

Moreover, using $V_{STZ} \approx 320 V_c$ together with Eq. **8**, we obtain a relation between the activation volume and the characteristic volume V_c given by $\Delta V \approx \sqrt{480}\ V_c$. With the values for V_c from the viscosity fitting, we can calculate the activation volume for the corresponding alloys to be in the range $151 - 324\ \mathring{A}^3$. For a Pd-based metallic glass, an activation volume of $106\ \mathring{A}^3$ was found experimentally (34), which is not too far from our estimate for the alloys discussed here.

Elsewhere the activation volume for $Zr_{41.2}\ Ti_{13.8}\ Cu_{12.5}\ Ni_{10}\ Be_{22.5}$ is determined to be $75\ \mathring{A}^3$ (35). For the same alloy, we calculate the value for the activation volume from the corresponding V_c with the result $\Delta V = 186\ \mathring{A}^3$, which is about 2.5 times larger in comparison. This difference may be explained by the different deformation protocols (shear amplitude, applied stress rate, etc.) in the respective experiments. It is argued in refs. 36 and 37 that a higher degree of applied stress leads to an increase of the size of the individual flow units, which means that both the STZ volume and the activation volume tend to increase.

Conclusions

The basic mechanism controlling the mechanical response and the fragility of liquid metals close to vitrification can be summarized in the following way. Due to thermal expansion, an increase in the temperature leads to a decreasing atomic packing fraction and, thus, to a decrease of atomic connectivity.

The latter effect softens the material, causing the shear modulus to decrease with T. The rate of this process is controlled by the steepness of the repulsive short-range interatomic interaction. This mechanism propagates to the viscosity, and it controls its temperature dependence and leads to fragile behavior with steep interatomic repulsion and to strong glasses when the repulsion is softer. In an amorphous solid we can picture this situation by considering a reference atom which is surrounded by a number of neighboring atoms, forming a disordered cage. The repulsive interaction between these particles provides stability to the cage. When the temperature is increased, a corresponding change of packing fraction takes place, implying that the disordered cage around the reference atom becomes larger and less stable (Fig. 4).

With this moving farther apart of the nearest neighbors from the reference atom, the local stabilizing energy felt by the atoms decreases due to a smaller overlap of the repulsive interatomic interactions by ΔE. At the onset of the glass transition, the stabilizing effect of the atomic cage breaks down, which ultimately leads to the vanishing of the zero-frequency shear modulus at T_g. It is the steepness of the repulsive pseudopotential which controls how rapidly or abruptly the stabilizing energy decreases as the temperature is increased. For an alloy whose constituents exhibit a steeper interatomic repulsion, this process of destabilization will be more abrupt, resulting in a faster variation of the shear modulus and viscosity with T and, correspondingly, to a more fragile glass.

We also show that the steepness of the interatomic repulsion for various metallic alloys can be mapped one-to-one onto a pseudopotential with two contributions. The overall softness of the pseudopotential is mainly controlled by Born–Mayer repulsion stemming from the overlap of valence shell electrons. A direct relation of linear proportionality between the fragility index m and the Born–Mayer energy B is obtained from the fitting to experimental data. Lower values of B may correlate with mixtures of elements having outer electrons in d-shells, as is the case of Cu in Zr-Cu alloys, or with the concentration of metalloid in metal–metalloid mixtures. Systematic studies in the future using ab initio simulations may shed light on the link with the detailed electronic structure.

Furthermore, we connect the characteristic atomic volume V_c with the size of STZs. In this regard, STZs appear to be regions in the amorphous solid with a relatively low average atomic connectivity Z. These regions are prone to elastic stress accumulation, leading to an increase in individual shoving events, which eventually results in macroscopic plasticity.

Although there exists a clear linear relation between the fragility and the repulsive steepness λ, the correlation between the size of a STZ and the fragility exhibits no simple form and remains to be understood in future investigations. We believe that the present framework may open up the possibility, in future work, of a priori designing metallic glasses with tailored rheological and mechanical properties (e.g., plasticity and ductility) (38) based on the alloy elemental composition.

ACKNOWLEDGMENTS. The support of the Technische Universität München Institute for Advanced Study, funded by the German Excellence Initiative and the European Union 7th Framework Programme under Grant Agreement 291763, is acknowledged.

1. Na JH, et al. (2014) Compositional landscape for glass formation in metal alloys. *Proc Natl Acad Sci USA* 111(25):9031–9036.
2. Bennett C, Polk D, Turnbull D (1971) Role of composition in metallic glass formation. *Acta Metall* 19(12):1295–1298.
3. Hafner J (1987) *From Hamiltonians to Phase Diagrams*, Springer Series in Solid-State Sciences (Springer, Berlin), Vol 70.
4. Götze W (2009) *Complex Dynamics of Glass-Forming Liquids: A Mode-Coupling Theory* (Oxford Univ Press, Oxford).
5. Mattsson J, et al. (2009) Soft colloids make strong glasses. *Nature* 462(7269):83–86.
6. Sengupta S, Vasconcelos F, Affouard F, Sastry S (2011) Dependence of the fragility of a glass former on the softness of interparticle interactions. *J Chem Phys* 135(19):194503.
7. Liu S, Wang Z, Peng H, Yu H, Wang W (2012) The activation energy and volume of flow units of metallic glasses. *Scr Mater* 67(1):9–12.
8. Lemaître A, Maloney C (2006) Sum rules for the quasi-static and visco-elastic response of disordered solids at zero temperature. *J Stat Phys* 123(2):415–453.
9. Zaccone A, Terentjev EM (2013) Disorder-assisted melting and the glass transition in amorphous solids. *Phys Rev Lett* 110(17):178002.
10. Dasgupta R, Joy A, Hentschel H, Procaccia I (2013) Derivation of the Johnson-Samwer $T^{2/3}$ temperature dependence of the yield strain in metallic glasses. *Phys Rev B* 87(2): 020101.
11. Alexander S (1998) Amorphous solids: Their structure, lattice dynamics and elasticity. *Phys Rep* 296(2-4):65–236.
12. Zaccone A, Schall P, Terentjev EM (2014) Microscopic origin of nonlinear nonaffine deformation in bulk metallic glasses. *Phys Rev B* 90(14):140203.
13. Born M, Huang K (1954) *Dynamical Theory of Crystal Lattices* (Oxford Univ Press, Oxford).
14. Zaccone A, Scossa-Romano E (2011) Approximate analytical description of the nonaffine response of amorphous solids. *Phys Rev B* 83:184205.
15. Ashcroft NW, Mermin ND (1976) *Solid State Physics* (Holt, Rinehart and Winston, New York).
16. Frenkel YI (1955) *Kinetic Theory of Liquids* (Dover, New York).
17. Lüthi B (2005) *Physical Acoustics in the Solid State, Solid State Sciences* (Springer, Berlin), Vol 148.
18. March NH (2005) *Liquid Metals: Concepts and Theory* (Cambridge Univ Press, Cambridge, UK).
19. Johnson WL, Demetriou MD, Harmon JS, Lind ML, Samwer K (2007) Rheology and ultrasonic properties of metallic glass-forming liquids: A potential energy landscape perspective. *MRS Bull* 32(8):644–650.
20. Wang WH (2012) The elastic properties, elastic models and elastic perspectives of metallic glasses. *Prog Mater Sci* 57(3):487–656.
21. Tobolsky A, Powell RE, Eyring H (1943) Elastic-viscous properties of matter. *Front Chem* 1:125–190.
22. Eyring H (1936) Viscosity, plasticity, and diffusion as examples of absolute reaction rates. *J Chem Phys* 4(4):283–291.
23. Dyre JC (1998) Source of non-Arrhenius average relaxation time in glass-forming liquids. *J Non-Cryst Solids* 235-237:142–149.
24. Dyre J (2006) Colloquium: The glass transition and elastic models of glass-forming liquids. *Rev Mod Phys* 78(3):953–972.
25. Angell CA, Ngai KL, McKenna GB, McMillan PF, Martin SW (2000) Relaxation in glassforming liquids and amorphous solids. *J Appl Phys* 88(6):3113–3157.
26. Bordat P, Affouard F, Descamps M, Ngai KL (2004) Does the interaction potential determine both the fragility of a liquid and the vibrational properties of its glassy state? *Phys Rev Lett* 93(10):105502.
27. Finnis M (2003) *Interatomic Forces in Condensed Matter* (Oxford Univ Press, Oxford).
28. Mott NF, Jones H (1958) *The Theory of the Properties of Metals and Alloys* (Courier Dover, New York).
29. Torrens IM (1972) *Interatomic Potentials* (Academic Press, New York).
30. Samwer K, Löhneysen Hv (1982) Amorphous superconducting Zr_x Cu_{1-x}: Electronic properties, stability, and low-energy excitations. *Phys Rev B* 26(1):107–123.
31. Egami T (2002) Nano-glass mechanism of bulk metallic glass formation. *Mater Trans* 43(3):510–517.
32. Li L, Homer E, Schuh C (2013) Shear transformation zone dynamics model for metallic glasses incorporating free volume as a state variable. *Acta Mater* 61(9):3347–3359.
33. Johnson WL, Samwer K (2005) A universal criterion for plastic yielding of metallic glasses with a (T/Tg) 2/3 temperature dependence. *Phys Rev Lett* 95(19):195501.
34. Heggen M, Spaepen F, Feuerbacher M (2005) Creation and annihilation of free volume during homogeneous flow of a metallic glass. *J Appl Phys* 97(3):033506.
35. Schuh C, Hufnagel T, Ramamurty U (2007) Mechanical behavior of amorphous alloys. *Acta Mater* 55(12):4067–4109.
36. Fan Y, Iwashita T, Egami T (2014) How thermally activated deformation starts in metallic glass. *Nat Commun* 5:5083.
37. Zhang M, Wang Y, Dai L (2015) Bridging shear transformation zone to the atomic structure of amorphous solids. *J Non-Cryst Solids* 410:100–105.
38. Kumar G, Neibecker P, Liu YH, Schroers J (2013) Critical fictive temperature for plasticity in metallic glasses. *Nat Commun* 4:1536.
39. Kato H, Chen H-S, Inoue A (2008) Relationship between thermal expansion coefficient and glass transition temperature in metallic glasses. *Scr Mater* 58(12):1106–1109.
40. Okumura H, Inoue A, Masumoto T (1993) Heating rate dependence of two glass transitions and phase separation for a La_{55} Al_{25} Ni_{20} amorphous alloy. *Acta Metall Mater* 41(3):915–921.
41. Waniuk T, Busch R, Masuhr A, Johnson W (1998) Equilibrium viscosity of the $Zr_{41.2}$ $Ti_{13.8}$ $Cu_{12.5}$ Ni_{10} $Be_{22.5}$ bulk metallic glass-forming liquid and viscous flow during relaxation, phase separation, and primary crystallization. *Acta Mater* 46(15):5229–5236.
42. Chen H (1978) Alloying effect on the viscous flow in metallic glasses. *J Non-Cryst Solids* 29(2):223–229.
43. Zaccone A, Blundell JR, Terentjev EM (2011) Network disorder and nonaffine deformations in marginal solids. *Phys Rev B* 84:174119.
44. Shannon RD (1976) Revised effective ionic radii and systematic studies of interatomic distances in halides and chalcogenides. *Acta Crystallogr A* 32:751–767.
45. Wang W, Dong C, Shek C (2004) Bulk metallic glasses. *Mater Sci Eng R Rep* 44(2-3):45–89.
46. Gaydaenko V, Nikulin V (1970) Born-Mayer interatomic potential for atoms with $Z = 2$ to $Z = 36$. *Chem Phys Lett* 7(3):360–362.
47. Faber TE (1972) *Introduction to the Theory of Liquid Metals* (Cambridge Univ Press, Cambridge, UK).
48. Abrahamson AA (1969) Born-Mayer-type interatomic potential for neutral ground-state atoms with $Z = 2$ to $Z = 105$. *Phys Rev* 178(1):76–79.
49. Dyre JC, Olsen NB, Christensen T (1996) Local elastic expansion model for viscous-flow activation energies of glass-forming molecular liquids. *Phys Rev B Condens Matter* 53(5):2171–2174.